Studies of Coupled Spin Systems

in the context of Supersolid behaviour in Solid Helium

A thesis submitted towards partial fulfillment of
BS-MS dual degree program
by

Sushant N More
Under the guidance of
Prof. Chandan Dasgupta
Dept. of Physics
Indian Institute of Science, Bangalore

Department of Physics
Indian Institute of Science Education and Research Pune

April 2011

Certificate

This is to certify that this dissertation entitled 'Studies of Coupled Spin Systems in the context of supersolid behaviour is solid Helium' submitted towards the partial fulfillment of the BS-MS dual degree programme at the Indian Institute of Science Education and Research, Pune represents original research carried out by Sushant N More at Dept. of Physics, Indian Institute of Science, Bangalore under the supervision of Prof. Chandan Dasgupta during the academic year 2010-2011.

Signature of student:

Supervisor:	Head Physical Sciences:
Date:	Date:
Place: Bangalore	Place: Pune

Acknowledgements

It is a pleasure to thank Prof. Chandan Dasgupta for agreeing to supervise my master's thesis and guiding me through it. It has been a privilege to work with him for the past two semesters. Among other things, he taught me to look at the numerical results with a physical insight. His invitation to IISc also opened for me doors to various academic and non-academic activities in and around IISc, which I immensely relished.

I am grateful to Dr. Arijit Bhattacharyay for consenting to be my local mentor at IISER, Pune and his constant support and motivation.

At IISc, I was fortunate to be surrounded by the best seniors a project student like me could aspire for. I am highly thankful to Sumilan for the numerous helpful discussions we had and admire his patience and knack of elucidating physical concepts. I am indebted to Subhro for parting with his bicycle which greatly facilitated my stay. Thanks are also due to my other lab mates - Kamil, Vishwanath and Kingshuk for their timely inputs and providing me an amicable atmosphere to work in.

Along with being enriching and educating, the last eight months also witnessed the most turbulent moments of my undergraduate life. I wish to express my heartfelt gratitude towards my friends - Sheetal, Sisir, Lakshmi Priya, Harsh and Lucky for standing besides me through thick and thin.

Finally, I must put on record the unremitting love and affection of my parents and sister which keeps me going.

Abstract

In recent years, there have been a lot of investigations, both experimental and theoretical of the possibility of simultaneous occurrence of crystalline order and superfluidity in solid helium. While there is still a lot of controversy about the microscopic mechanism of superfluidity in solid helium, there is increasing evidence that suggests that the superfluid component in this system resides primarily on structural defects such as dislocations and grain boundaries. In a three dimensional system, dislocations form a network of lines (one-dimensional objects) and grain boundaries form a network of two-dimensional planar objects. To study superfluidity on such networks, one first needs to construct realistic versions of the network.

In the coupled spin models that we study in this context, one of the spin systems is used to generate the network of defects. We then study the equilibrium and dynamic properties of the coupled spin systems using numerical and analytical techniques.

Contents

Chapter 1

Introduction and Motivation

1.1 Superfluidity in Helium

Superfluidity is a state in which matter behaves like a fluid without viscosity and with infinite conductivity. Thus a superfluid can flow by itself and can pass through extremely thin capillaries (known as superleaks). Due to its infinite thermal conductivity it is impossible to create temperature gradient in a superfluid.

Superfluidity was discovered by Allen, Misener and Kapitza in 1938 [1]. They observed that below a certain temperature (~ 2.17), the resistance of liquid helium to flow in narrow channels drops drastically. Superfluidity has been described both through phenomenological [2], [3] and microscopic theories [4], [5]. Superfluidity is observed both in Helium 4 as well as Helium 3. However the underlying physics in the two cases is completely different. Superfluidity in Helium 4 can be regarded as Bose- Einstein condensation in an interacting system. Helium 3 atoms on the other hand are fermions. Superfluidity in this case is explained by a generalization of BCS theory of superconductivity wherein the Helium 3 atoms form Cooper pairs.

Superfluidity opens exciting avenues of intellectual and industrial interests. The properties of superfluid state have been extensively studied and have been understood to a great deal in terms of microscopic physics. The reader may refer [1], [6] for a detailed description of this intriguing field.

1.2 The enigma of supersolidity

A solid with superfluid properties is called 'supersolid'. A supersolid phase combines both crystalline properties such as shear modulus and broken translational symmetry, with frictionless mass transport of its own atoms through the solid bulk.

Helium at ordinary pressure does not go into solid form. However it can be solidified by applying high pressures. Chester conjectured in 1970 that Helium 4 might undergo a transition to a supersolid phase [7]. The experiments performed by Kim and Chan in 2004, is believed to show signatures of supersolidity in Helium [8], [9]. Figure 1.1 depicts the phase diagram of Helium indicated by them in [9]. Kim and Chan's conclusion was based on the observed anomaly in the rotational

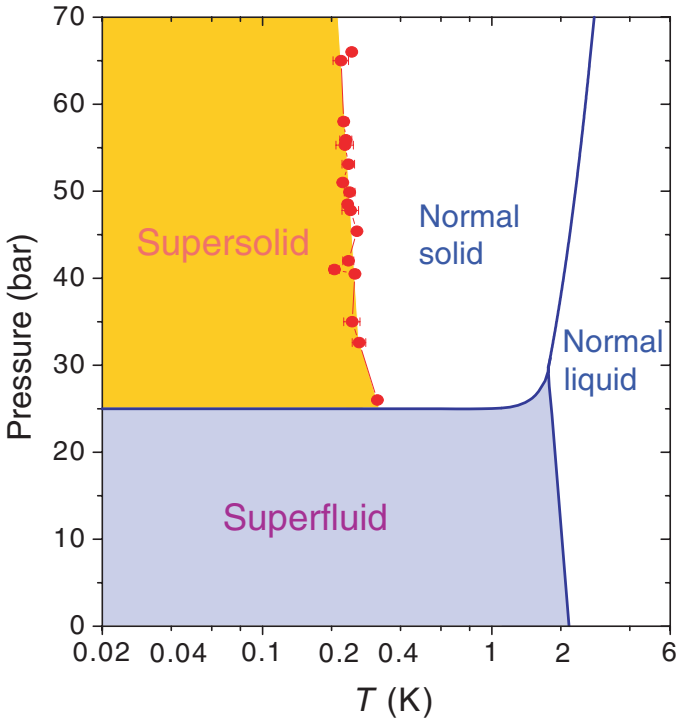

Figure 1.1: The phase diagram of Helium below 6 K as reported in [9].

properties of solid Helium. Their conclusion has been contended as to if the so called supersolid state exists at all [10]. But since then a number of experiments have been performed which report anomalies not only in the rotational properties of solid Helium but also in its elastic properties [11], [12] and in its specific heat [13]. Following these reports there has been a general consensus within the scientific community that supersolid state does exist. However, the mechanism behind the formation of supersolidity is extensively debated.

As pointed out in [14] a model for supersolidity was proposed by Thouless and by Andreev and Lifshitz in [15] and [16] respectively, where they consider a quantum crystal with vacancies. The vacancies could exchange their positions with neighbouring atom through quantum tunneling. If atoms are bosons, the mobile vacancies obey Bose- Einstein statistics and undergo Bose-Einstein condensation, below a particular temperature. Since, flow of vacancies is inverse the flow of mass, we could observe a fraction of the mass flowing without friction through the lattice, which characterizes a supersolid. The flaw in this argument being that the ansatz of existence of vacancies in zero temperature limit is not well justified.

1.2.1 The role of disorder

As described above, the emergence of supersolidity entails existence of vacancies in the ground state of Helium. Monte Carlo studies indicate [17], [18] that creation of vacancies in ground state would require large energy casting a doubt over vacancy

based model of supersolidity.

Rittner and Reppy [19] established that in annealed crystal samples with very low defect density the supersolidity signal decreases sharply and falls within the noise levels in measurements. They were also able to reproduce the Kim and Chan's results [8], [9] with the normal crystals. Further, most Helium 4 samples invariably contain small amount of Helium 3. The supersolid transition depends sensitively on the concentration of Helium 3 impurities. It has been shown that the transition temperature decreases monotonically with the reduction of Helium 3 concentration [20]. Thus supersolid transition is highly influenced by disorder. However, the actual role of disorder remains a moot point. While some believe that supersolidity is solely driven by defects and impossible in a perfect crystal [17], Anderson [21] maintains that supersolidity is the intrinsic property of ideal crystal which is only enhanced by disorder. Moreover, the nature of disorder which leads to the observed supersolid properties and the mechanism by which it does so, remains unclear [22]. Presently, experimental and theoretical work continues with the hope to unveil the mystery of supersolidity.

1.3 The Project Outline

We began with the study of coupled Ising Models. One of the Ising spins form the domains and the coupling between the second Ising variables is decided by whether they lie across the domains of former or not. The mean field and Monte Carlo study of this model is presented in Chapter 2. We observe that Ising spins do not order along the one dimensional Ising domain boundaries and this motivates us to consider a 3 state Potts Model whose domain boundaries form a network in two dimensions.

Chapter 3 is devoted to the study of Potts Model and the ordering of Ising spins along the domain boundaries of Potts spins. We also report an estimate of critical temperature for ordering of Ising spin along such a network.

In chapter 4 we present our numerical and analytical endeavours to understand the effect of dynamics of the underlying network on the ordering of spins. We conclude with a discussion of the results obtained and deliberate over the scope of further developments.

Chapter 2

Coupled Ising Models

2.1 The Model

We embark on our study of coupled spin systems in the context mentioned in 1.2.1 by considering the case of two coupled Ising variables, S and σ. The σ spins form the domains and the coupling between the S spins is decided by their position. If the S spins lie along the domain boundaries of σ spins they are assigned a coupling constant of say J_2, different from the case, when they lie within the σ domains, say J_3. The Hamiltonian of such system would be,

$$H = -J_1 \sum_{<i,j>} \sigma_i \sigma_j - \sum_{<i,j>} \tilde{J}(\sigma_i, \sigma_j) S_i S_j \tag{2.1}$$

where,

$$\begin{aligned} \tilde{J}(\sigma_i, \sigma_j) = & \quad J_2 \delta_{\sigma_i \sigma_j, -1} + J_3 \delta_{\sigma_i \sigma_j, +1} \\ = & \quad \tfrac{J_2}{2}(1 - \sigma_i \sigma_j) + \tfrac{J_3}{2}(1 + \sigma_i \sigma_j) \\ = & \quad \tfrac{J_2 + J_3}{2} - \tfrac{J_2 - J_3}{2} \sigma_i \sigma_j \end{aligned}$$

So, equation (2.1) becomes,

$$H = -J_1 \sum_{<i,j>} \sigma_i \sigma_j - \sum_{<i,j>} \frac{J_2 + J_3}{2} S_i S_j + \sum_{<i,j>} \frac{J_2 - J_3}{2} \sigma_i \sigma_j S_i S_j$$

Considering $J_3 = 0$, the Hamiltonian reads as,

$$H = -J_1 \sigma_i \sigma_j - \frac{J_2}{2} S_i S_j + \frac{J_2}{2} \sigma_i \sigma_j S_i S_j \tag{2.2}$$

The equation(2.2) is similar to the Hamiltonian for Ashkin Teller Model studied in [23], [24] and [25]. Taking clues from these, we employ mean field and numerical techniques to understand the phase diagram of system governed by Hamiltonian (2.2)

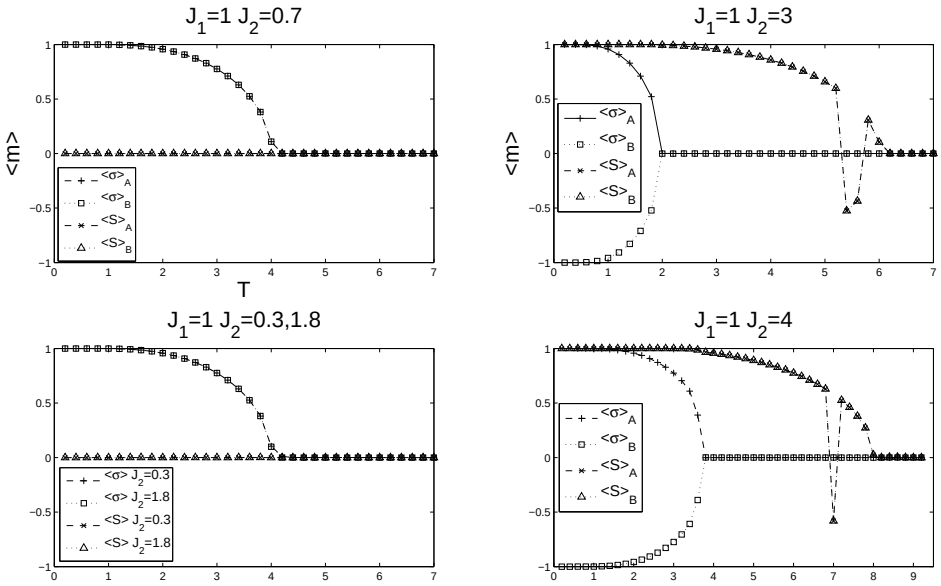

Figure 2.1: The mean field magnetization versus temperature graphs for various values of J_2

2.2 Mean Field treatment

To include the possibility of antiferromagnetism, we consider two sublattices, A and B and calculate the magnetization of σ and S in these two sublattices. Please refer Appendix A.1 for a brief note on set up of mean field equations.

The four self consistent mean field equations are,

$$\langle\sigma\rangle_A = tanh(\frac{4J_1\langle\sigma\rangle_B - 2J_2\langle S\rangle_A\langle S\rangle_B\langle\sigma\rangle_B}{k_BT}) \tag{2.3a}$$

$$\langle\sigma\rangle_B = tanh(\frac{4J_1\langle\sigma\rangle_A - 2J_2\langle S\rangle_A\langle S\rangle_B\langle\sigma\rangle_A}{k_BT}) \tag{2.3b}$$

$$\langle S\rangle_A = tanh(\frac{2J_2\langle S\rangle_B - 2J_2\langle\sigma\rangle_A\langle\sigma\rangle_B\langle S\rangle_B}{k_BT}) \tag{2.3c}$$

$$\langle S\rangle_B = tanh(\frac{2J_2\langle S\rangle_A - 2J_2\langle\sigma\rangle_A\langle\sigma\rangle_B\langle S\rangle_A}{k_BT}) \tag{2.3d}$$

Without loss of generality we can put $J_1 = 1$ We use the subroutine discussed in [26] to solve the above equations. The main observations which can be made from Figure 2.1 are as follows,

- For $J_2 < 2J_1$, the σ spins are ordered ferromagnetically till a temperature of 4 (temperature is measured in units of J_1)
- For $J_2 > 2J_1$, at low temperatures, the σ spins are ordered antiferromagnetically and S spins are ordered ferromagnetically. The anti-ferromagnetic order

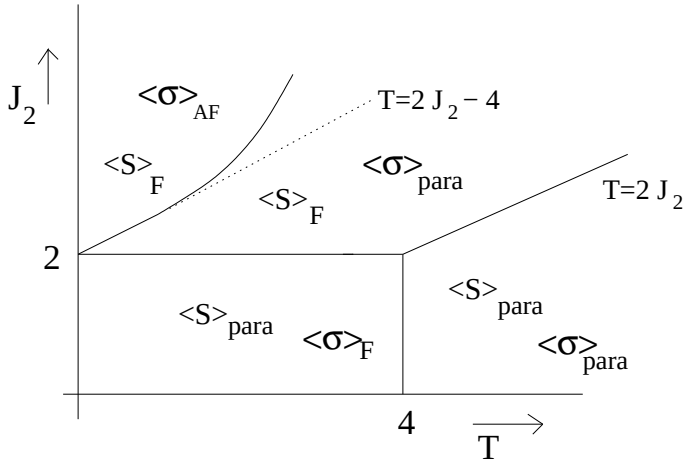

Figure 2.2: The mean field phase diagram of the coupled Ising model. Both J_2 and T are expressed in units of J_1.

breaks at a $T = 2J_2 - 4$ and the ferromagnetic order breaks at $T = 2J_2$.[1]

We also observe that at high J_2 values, the antiferromagnetic order of σ spins break at a temperature lower than $2J_2 - 4$.

These considerations, lead us to a phase diagram as shown in Figure 2.2

2.3 Numerical Results

In this section, we present the numerical results of the Monte Carlo simulations of our coupled Ising system.

In the first set of simulations, we fix temperature and look at behaviour of the order parameters - $\langle\sigma\rangle_{AF}$, $\langle\sigma\rangle_F$ and $\langle S\rangle_F$ as the coupling constant J_2 is varied. A few such graphs are shown in Figure 2.3.

In the second set of simulations, we fix J_2 and study the magnetization order parameter as a function of temperature. Figure 2.4 gives a few such plots. The observations of simulations lead us to construct a phase diagram as show in Figure 2.5.

2.3.1 Ordering along domain boundaries

We are interested in dynamics of S spins along the domain boundaries of σ spins. In Figure 2.5, we set the parameters such that we are in the phase, where $\langle\sigma\rangle$ is ferromagnetically ordered. Once, we have some domain formation of σ spins, we freeze them and update only S spins.

A result of such exercise is shown in Figures 2.6 and 2.7. It is seen that S spins lying along the domain boundary do not show any tendency to develop magnetic

[1] In case of two sublattices, the ferromagnetic and antiferromagnetic order parameters are defined as $\langle\sigma\rangle_F = (\langle\sigma\rangle_A + \langle\sigma\rangle_B)/2$ and $\langle\sigma\rangle_{AF} = (\langle\sigma\rangle_A - \langle\sigma\rangle_B)/2$

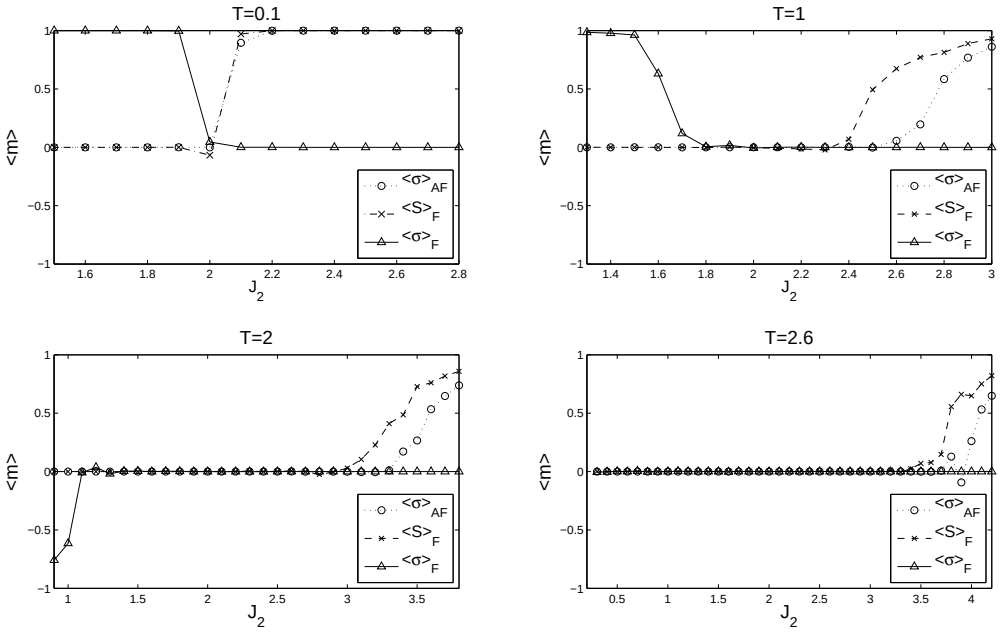

Figure 2.3: The magnetization versus J_2 graphs for various values of temperatures. $J_1 = 1$

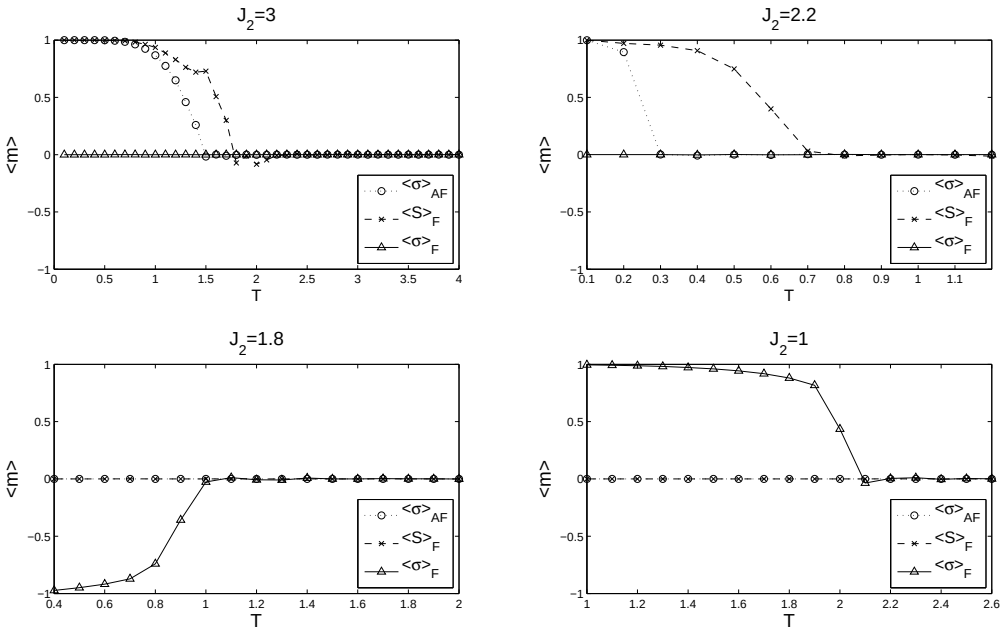

Figure 2.4: The magnetization versus temperature graphs for various values of J_2. $J_1 = 1$

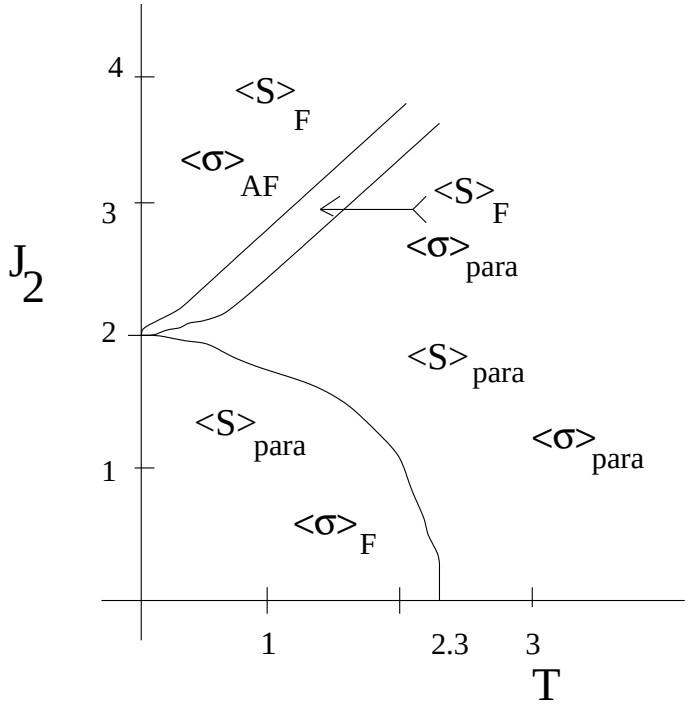

Figure 2.5: The phase diagram of a coupled Ising Model (equation (2.2)) from Monte Carlo Simulations.(Both J_2 and temperature are measured in units of J_1)

order. This is expected as it is known that Ising variables do not order at any finite temperature in one dimension. The domain walls of a two dimensional Ising Model is one dimensional and hence no order is seen along the domain boundary.

Starting with patched initial condition

Instead of starting with a random initial configuration for σ spins, we start with an initial configuration wherein we have blocks of spins pointing in one direction and the adjacent blocks of spins, point in the opposite direction.

This patched initial configuration, is evolved over a few Monte Carlo steps. The domain boundaries, rather than being simply one dimensional as in earlier case, have a few connections and form network-like patterns. We now see if the spins order along these domain boundaries.

Figure 2.8 shows a domain diagram on starting from such patched initial configuration. From Figure 2.9, we see that even in this case, the S spins along the domain boundaries do not order. The Monte Carlo evolution destroys the network structure of domain boundaries and makes them essentially one dimensional.

The above studies, make it clear that in two dimensions we cannot get order along the domain boundaries formed by coupled Ising Models. These results motivate us to consider the ordering of spins along a network. These studies are described in next chapter wherein we use a three states Potts Model to form the underlying network and the ordering of Ising spins along such a network is studied.

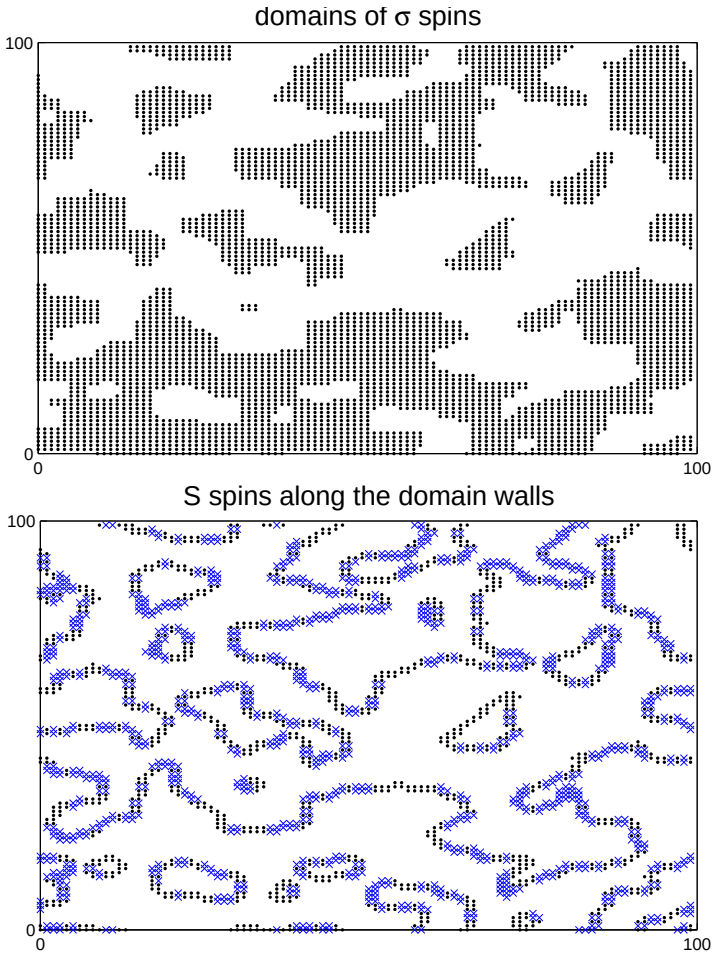

Figure 2.6: The top figure: shows the arrangement of σ spins after the system (Equation (2.2)) is evolved over 200 Monte Carlo steps starting with random initial configuration. The $\sigma = 1$ spins are indicated by black dots. The absence of black dot implied the presence of $\sigma = -1$ spin. $J_2 = 1.2$, $T = 0.4$, MC steps $= 200$.
The bottom figure: show a snapshot of S spins along the domain boundaries of σ spins after 10000 MC steps over S spins (keeping the σ spins fixed) The up and down spins are indicated by $\bullet$ and x respectively.

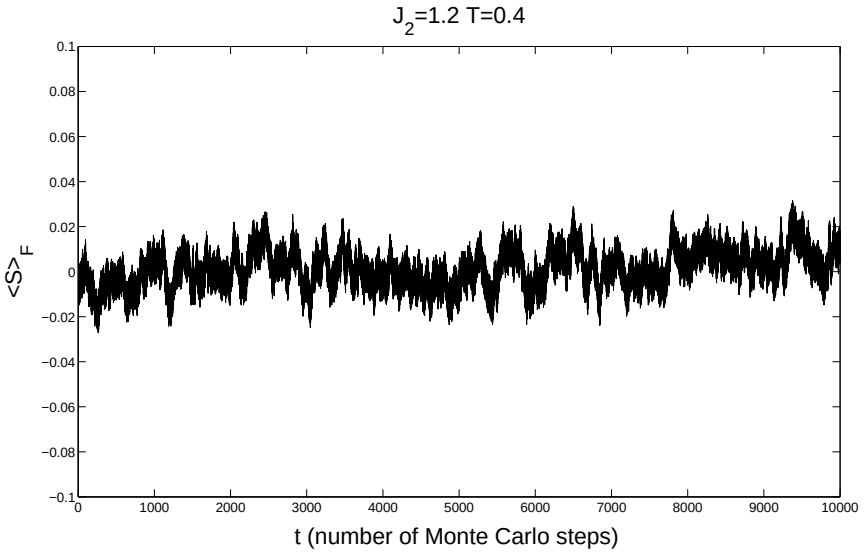

Figure 2.7: The magnetization of S spins as a function of time, when the domains of σ spins are frozen in time. We observe that the S spins do not develop any order over time.

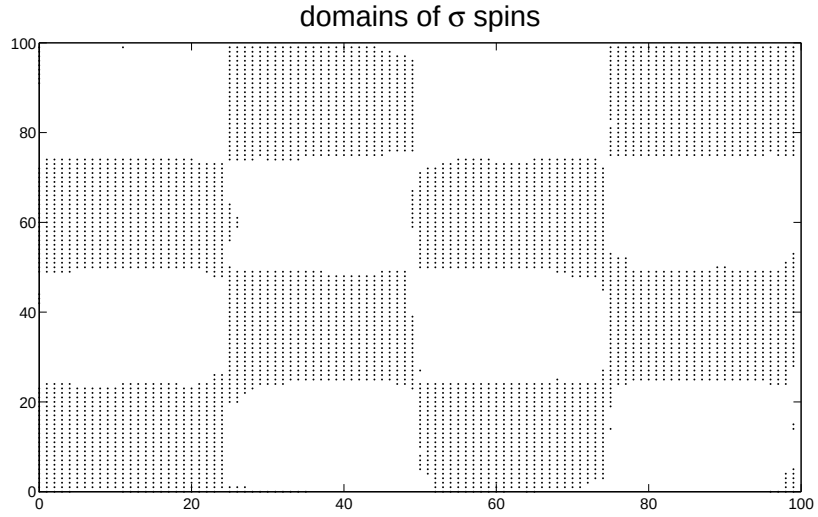

Figure 2.8: The σ domains starting from a patched initial configuration. MC steps $= 40$, $J_2 = 1.2$, $T = 0.4$

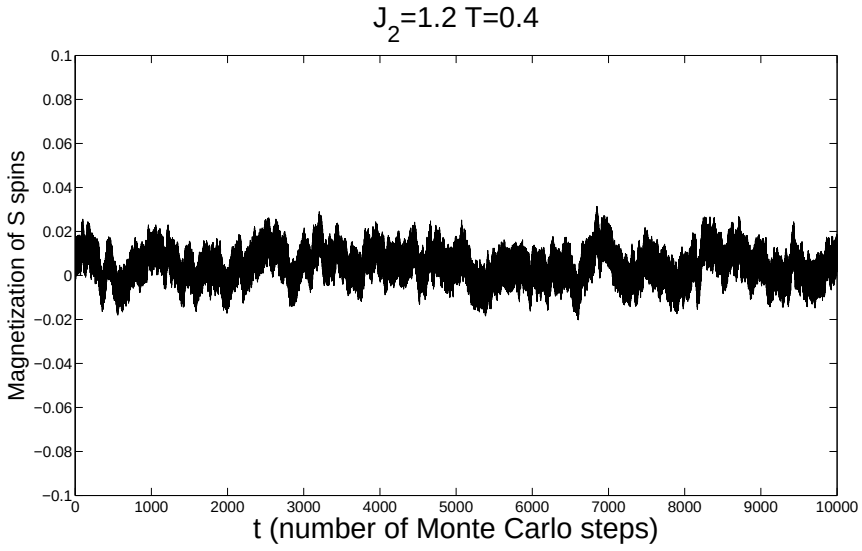

Figure 2.9: The magnetization of S spins along the domain boundaries of σ spins (Figure 2.8). Even in this case, the S spins do not develop any order over time.

Chapter 3

Coupled Potts Ising Model

3.1 The Potts Model

The Hamiltonian of the standard Potts Model [28] is given

$$\mathcal{H} = -J \sum_{\langle i,j \rangle} \delta(S_i, S_j) \tag{3.1}$$

In a q state Potts Model, the spin on the lattice can take q different values, contributing non-zero energy only when the neighbouring spins are in the same state. It is easy to see that a two state Potts Model ($q = 2$) is an Ising Model with shifted energy scale.

The Potts Model has been extensively studied and many of its properties are known [29]. The critical temperature of Potts Model in two dimensions on a square lattice is given by [30]

$$T_c = \frac{2J}{k_B ln(1 + \sqrt{q})} \tag{3.2}$$

Note that $q = 2$, reproduces $T_c \sim 2.269$, the critical temperature of two dimensional Ising Model [31] (with $J = k_B = 1$).

Figure 3.1 shows a domain formation in a 3 state and a 4 state Potts Model. It also shows the spins lying along the domain boundaries. These spins form a network, in contrast to simple one dimensional lines as in coupled Ising Model case. It would be interesting to study if any ordering occurs along such a network. This is our agenda in the rest of this chapter. We study the ordering of an Ising variable in network geometry formed by the domain boundaries of Potts spins.

3.2 Ising Spins along the network

In this section, we study the ordering of Ising spins along the network shown in Figure 3.1 C). We consider the Ising spins, S over a square lattice. Only those spins which lie along the network are coupled whereas the rest are not coupled. The uncoupled spins on an average would add up to zero and will not contribute to net magnetization. So, it suffices to study the behaviour of coupled spins.

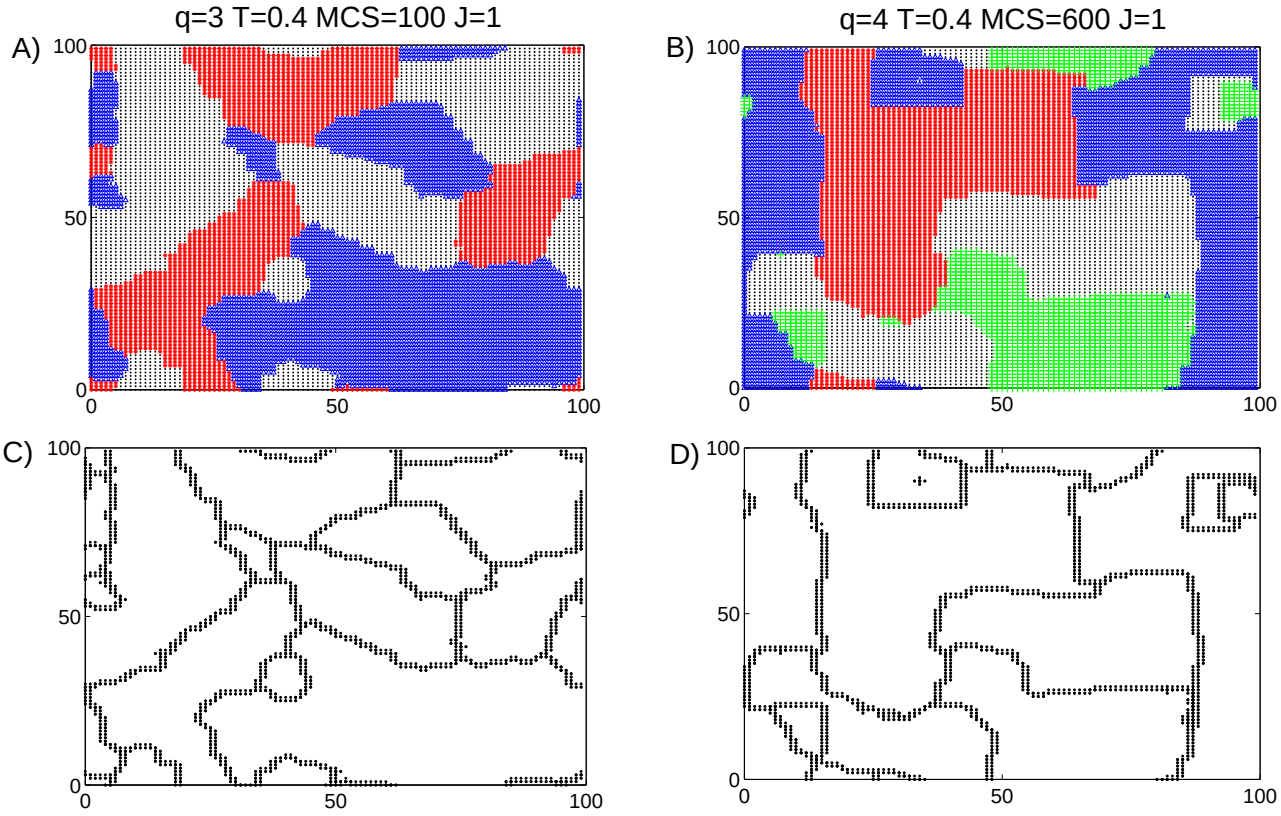

Figure 3.1: A)The domain formation in a 3 state Potts Model after 100 Monte Carlo steps at $T = 0.4$ and coupling constant, $J = 1$ starting with a random initial configuration.
B)The domain formation in a 4 state Potts Model after 600 Monte Carlo steps at $T = 0.4$, $J = 1$ starting with a random initial configuration.
C)The spins that lie along the domain boundary of 3 state Potts Model
D)The spins that lie along the domain boundary of 4 state Potts Model

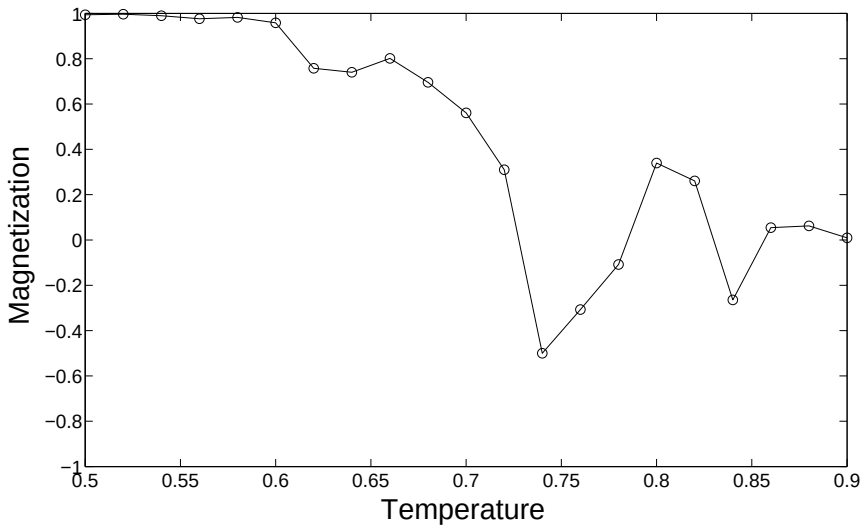

Figure 3.2: The magnetization of Ising spins, S as a function of Temperature. The coupling constant of spins lying along the network,$J = 1$.

Figure 3.2 shows that the S spins [1] order along the network at low temperatures. This ferromagnetic order breaks down as the temperature is increased. The temperature, at which the S spins cease to remain ordered, defines the critical temperature, T_c of this system.

3.2.1 Calculation of T_c

The accurate estimation of T_c for such a geometry is a formidable task. Nonetheless, with the limited time and computational resources we have we try to get a good estimate of the critical temperature. It is difficult to get a good estimate of T_c by just looking at the magnetization with respect to temperature as in Figure 3.2 because,

- The spins get stuck in meta-stable domains.
- The system being finite sized, flips over long runs from positive magnetization to negative magnetization. Averaging over all such values of magnetizations gives us a wrong estimation of the thermodynamic average.

Therefore, we choose to look at the susceptibility χ,[2] which is a measure of fluctuations in the magnetization. The susceptibility is expected to be sharply peaked at the critical temperature.

Figure 3.3 leads us to conclude that the critical temperature of Ising spins on the network geometry is close to 0.72.

[1] Here onwards, for brevity we shall refer to Ising spins as S spins

[2] $\chi = \frac{\langle m^2 \rangle - \langle m \rangle^2}{T}$, where m is the magnetization of the system

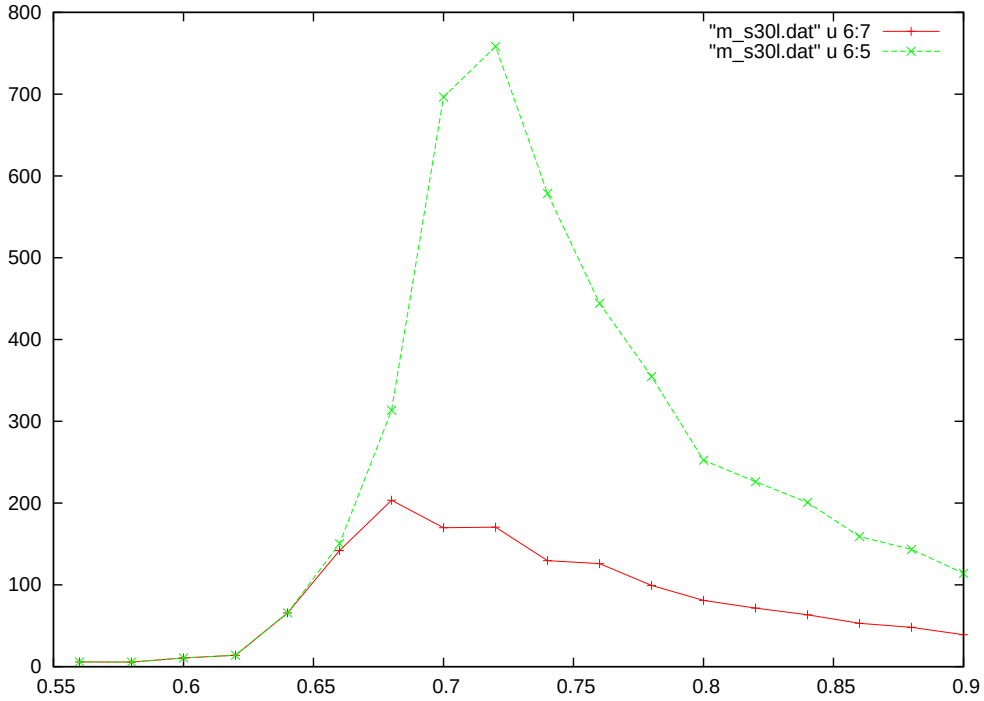

Figure 3.3: The susceptibility as a function of temperature. The graph which peaks at a lower value represents $\chi_{mod} = \frac{\langle m^2 \rangle - \langle |m| \rangle^2}{T}$

The thermodynamic value of magnetization (or any other physical property of interest) at a given temperature is calculated by averaging over the individual magnetizations of all possible equilibrium configurations. The histogram of magnetization values, above T_c is a gaussian with a mean at zero. Below T_c, for a finite size system, we have a bi-modal distribution peaked at $-m$ and m, if m is the thermodynamics magnetization. Thus the histograms at various temperatures could offer us yet another estimate for the critical temperature of the system.

Figure 3.4 shows that at $T = 0.68$, the spins are ordered. Please note that if we allow sufficient time, so that the system undergoes multiple flips, then we would get a bi-modal distribution as discussed in above paragraph. Similarly, it is also clear from Figure 3.4 that $T = 0.78$ is a disordered state. Thus, we conjecture that the critical temperature, $T_c \sim 0.72$.

3.2.2 Behavior of specific heat

The specific heat at constant volume, C_v is an important response function which is vital in study of any system. In this subsection, we study the behaviour of specific heat of the Ising spins in our geometry.

Figure 3.5 shows that in this case the C_v vs T graph shows a rounded peak, rather than a sharp peak.

In Figure 3.5, we have calculated the specific heat using the formula, $C_v = \frac{\langle E^2 \rangle - \langle E \rangle^2}{T^2}$, where E is the energy. But we also have $C_v = \frac{\partial E}{\partial T}$. We calculate the

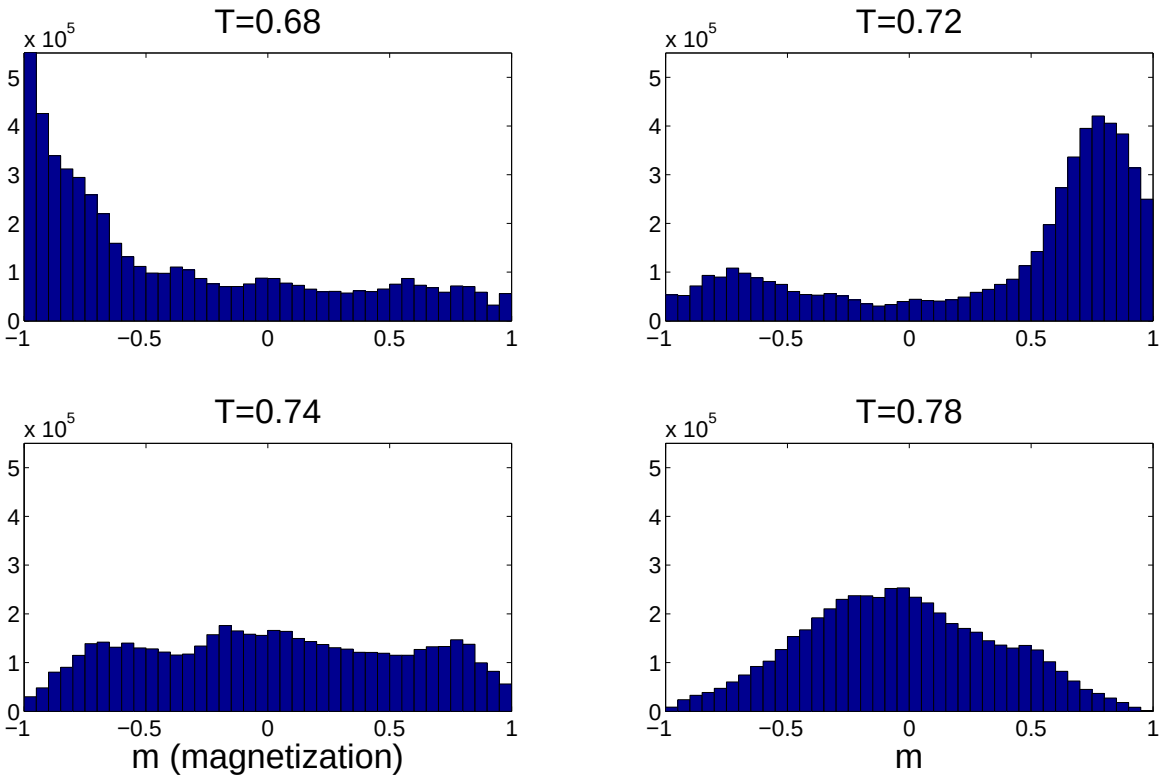

Figure 3.4: The histograms depecting the distribution of magnetization at various temperatures.

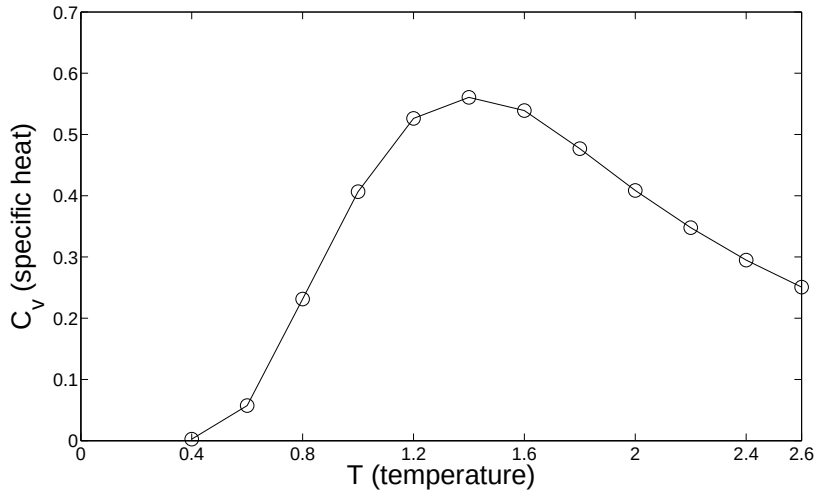

Figure 3.5: The specific heat as a function of temperature, shows a rounded peak.

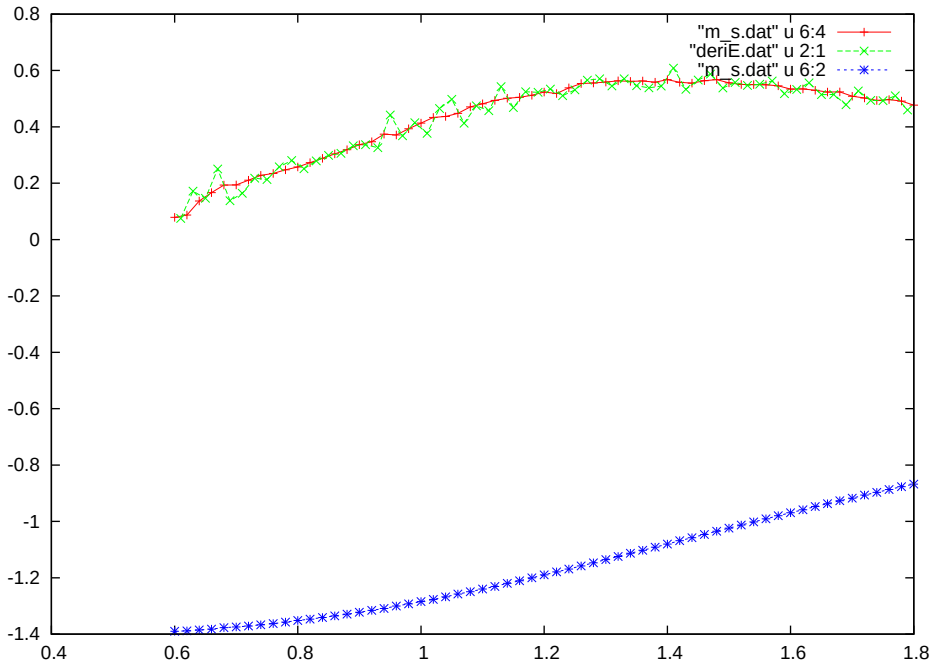

Figure 3.6: The specific heat as a function of temperature, calculated in two different ways. The blue line indicates the energy of the system at given temperature.

numerical derivative of energy with respect to temperature and compare it with our earlier result for C_v. From Figure 3.6, we see that the two methods give very close answers. This validates our calculation of C_v.

The specific heat behaviour seen in Figure 3.5 is quite similar to the specific heat of an one dimensional Ising chain as a function of temperature [32]. At high temperatures, the correlation length decreases and a given spin, does not see other spins beyond a few neighbours. Thus the system essentially behaves as one dimensional at high temperatures.

The specific heat for a linear Ising chain is given by,

$$C_v = Nk_B(\beta\frac{z}{2}J)^2 sech^2(\beta J\frac{z}{2}) \tag{3.3}$$

$$so, \quad C_v \sim (\frac{z}{2T})^2 sech^2(\frac{z}{2T}) \quad where, J = k_B = 1 \tag{3.4}$$

In equation (3.4), N is the total number of spins in the chain and z is the number of nearest neighbours which is two in 1D. According to the argument given above, the specific heat for our system should also follow a similar equation at high temperature. The only difference being that z in this case, will be different from 2 and will represent the average number of neighbours a spin has in the network geometry being considered.

We used the gnuplot fitting tool to fit the tail of C_v to Equation (3.4). For $T <= 2.2$, the best fit is obtained when the parameter z in the Equation (3.4) is equal to 2.8. This value is obtained within an error bar of ± 0.03.

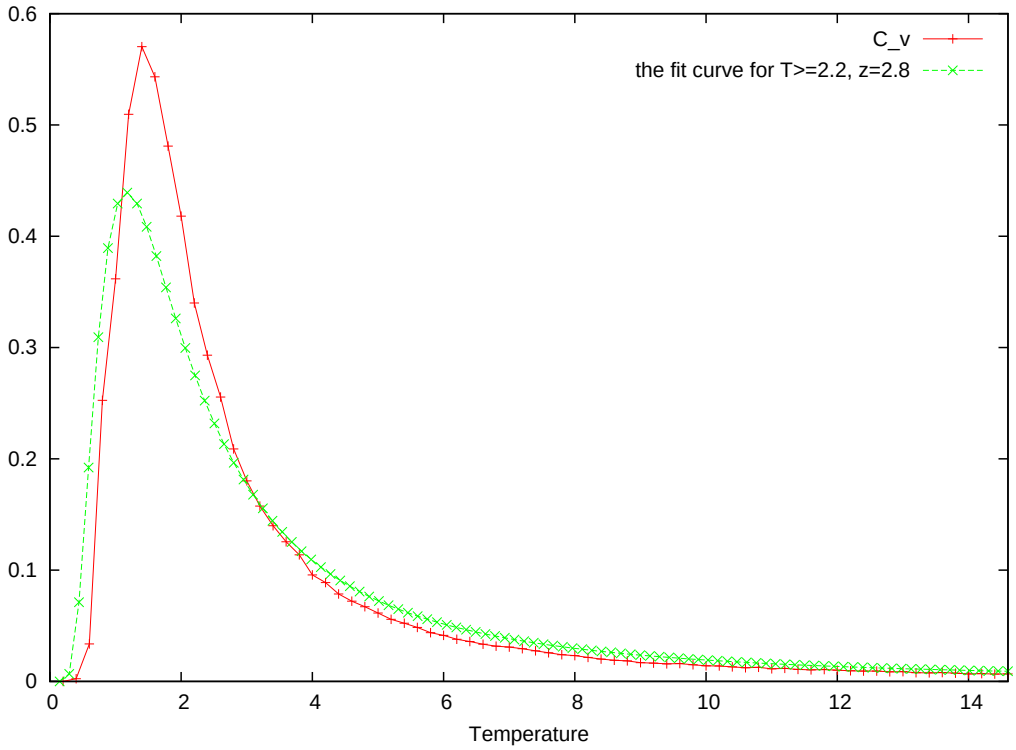

Figure 3.7: The tail of C_v best fits to the Equation (3.4) for $z = 2.8$.

The energy of the configuration, in which all spins are ordered along the same direction is -1.39. (This can also be seen from Figure 3.6). Thus the average number of nearest neighbours according to this is 2.78, which agrees well with the fit obtained in Figure 3.7.

Chapter 4

Ordering along a dynamic network

In the preceding chapter we have identified a network along which the Ising spins order ferromagnetically. We also have obtained some knowledge about the critical temperature and the behaviour of various thermodynamics quantities of the Ising spins along this network. We now embark upon the study of ordering in the spirit mentioned in Chapter 1.

In the first section of the chapter we present the results of our simulations. In the next section, we build up models which resemble our system and study them analytically.

4.1 Numerical approach

The temperature of the system is kept below T_c, estimated in the Chapter 3. We wish to compare the ordering along the network in two different scenarios.

1. The underlying Potts network is fixed and the Ising spins are updated using the Monte Carlo scheme for a certain number of Monte Carlo steps (which is a measure of time). Please note that only the Ising spins across the domain boundaries are coupled and contribute to the magnetization.

2. The same number of Monte Carlo updates as in 1. are done, but the Potts network is regularly updated. For example, say we choose to do N Monte Carlo updates over Ising spins in above case. In this case, if we choose to update the Potts network a times, then each update of Potts variables will be followed by N/a Monte Carlo updates of Ising spins. This way the total number of Monte Carlo steps for Ising spins remains the same in two cases.

We wish to know, in which of the two cases do spins have more tendency to order. Please note that in the second case, the Potts spins domain boundaries change after we update the Potts spins. Therefore, the Ising spins which are coupled to each other also need to be changed with every Potts update.

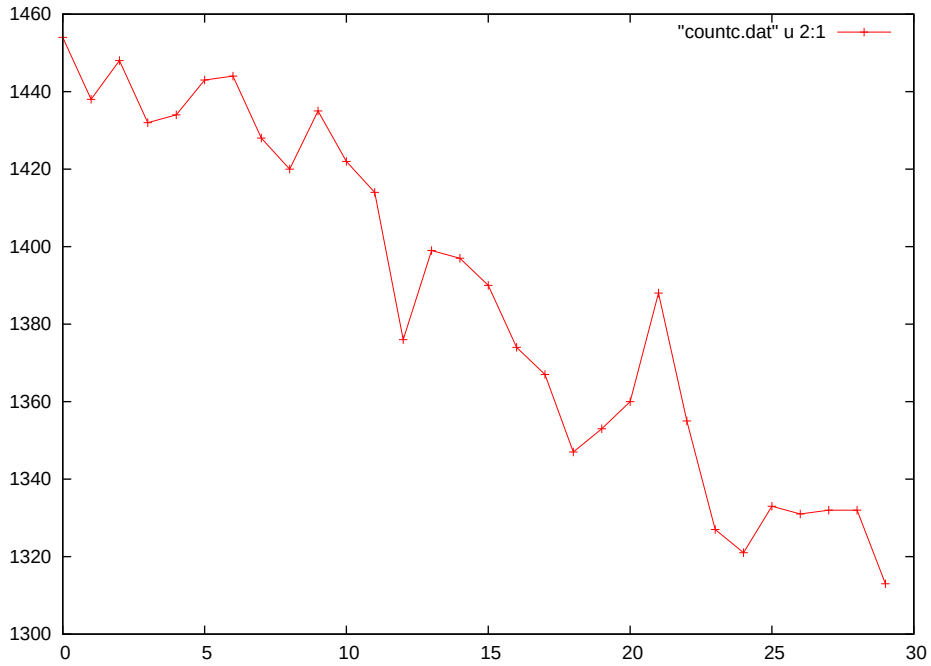

Figure 4.1: The number of Ising spins across the domain boundary of Potts spin decreases as the number of Monte Carlo updates over Potts spins is increased. The X axis gives the number of Monte Carlo updates over 100.

4.1.1 The Potts spin update

The network geometry which we had studied in the previous chapter was obtained by freezing (stopping further evolution) the dynamics of Potts spins after a few Monte Carlo steps (Figure 3.1C)). If further Monte Carlo updates of the Potts spins are done, the domains grow bigger in size until we are ultimately left with only one domain. This consideration makes us aware of a difficulty in implementing the second scheme discussed above. If the intermediary Potts updates are done following the usual Monte Carlo rule, the length of domain boundary decreases at every step and thus we have less number of coupled Ising spins at subsequent steps. (Figure 4.1) This would naturally lead to a lower magnetization in the dynamical network case. However, this is not the effect we are interested in studying.

To circumvent this problem, instead of following the usual Metropolis algorithm for acceptance, we choose to accept only those updates of the Potts spins which leave the energy unchanged. This ensures that the domain length remains the same and we can hope to see if any genuine differences exist in ordering between the fixed network and dynamical network case. Figure 4.2 shows a change in network as a result of such updates.

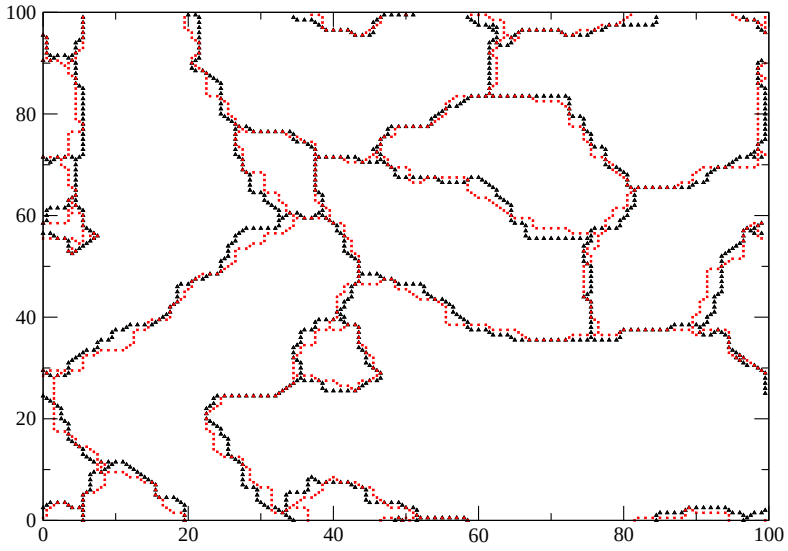

Figure 4.2: The change in network when the Potts spins are updated subject to the constraint that the energy remains fixed at each step.

4.1.2 Numerical results

We start with a network shown in Figure 3.1C. The parameters of Ising spins are set as $T = 0.58$ and $J = 1$. In the first case we evolve the Ising spins for 1 crore Monte Carlo steps. In the second case, the Potts spins are updated 40 times according to the method explained above and each update of Potts spins is followed by 250000 Monte Carlo updates over Ising spins. To get a good statistical description the complete process is repeated many number of times. The different successive runs correspond to a different realization of random number realization and give different values of the magnetization. The mean of these magnetization values is calculated for the moving network case and the fixed network case and compared. While comparing the means in two scenarios, we also need to know the error in the mean, so that we are able to make definite conclusions.

For N independent and identically distributed random variables, $X_1, \ldots X_N$ each with an expectation value μ and variance σ^2, the standard deviation of sample mean, $\bar{X}$ ($\bar{X} = \sum_{i=1}^{N} X_i/N$) is given by

$$std(\bar{X}) = \frac{\sigma}{\sqrt{N}} \tag{4.1}$$

A brief derivation of (4.1) is presented in Appendix B.1.

The mean value of magnetization ($\bar{M}$) and the error in the mean (given by standard deviation, $std(\bar{M})$) for the two cases is reported in Table 4.1.

Table 4.1: Simulation results ($T = 0.58$, $J = 1$)

Number of configurations, N	**Fixed network MCS=10000000**	**Dynamic network MCS=40×250000**
20	$\bar{M} = 0.9108$ $std(\bar{M}) = 0.0138$	$\bar{M} = 0.9166$ $std(\bar{M}) = 0.0088$
40	$\bar{M} = 0.9128$ $std(\bar{M}) = 0.0089$	$\bar{M} = 0.9104$ $std(\bar{M}) = 0.0085$
80	$\bar{M} = 0.91318$ $std(\bar{M}) = 0.00597$	$\bar{M} = 0.91719$ $std(\bar{M}) = 0.00527$

The analysis of these results is presented in the next chapter. However, note that the small difference in magnetization renders us incompetent to make a definite statement about the comparative tendency of ordering between the fixed and dynamic network case.

At this point, it would be helpful to analytically study a model which bears resemblance to our system. We hope that it could help us get better understanding of our system.

4.2 Analytical work

4.2.1 Linear double Ising chain

As remarked in 3.2.2, the network (Figure 3.1 C)) is essentially one dimensional if the spins do not see each other beyond a few sites. In that case, a spin picked at random will not see the network joints. So, we may model the system as a linear double Ising chain as in Figure 4.3. This double chain model can be solved using transfer matrix method. Spins on one of the chain are denoted by σ and on the other chain by S.We apply periodic boundary condition. The Hamiltonian of the system is given by,

$$\mathcal{H}_N(\sigma_i, S_i) = -J\sum_{n.n}\sigma_i\sigma_j - J\sum_{n.n}S_iS_j - J\sum_{n}\sigma_iS_i - \mu B\sum_{i=1}^{N}\sigma_i - \mu B\sum_{i=1}^{N}S_i \quad (4.2)$$

Putting it in a symmetrical form,

$$\begin{aligned}\mathcal{H}_N(\sigma_i, S_i) = -J\sum_{i=1}^{N}\sigma_i\sigma_{i+1} - J\sum_{i=1}^{N}S_iS_{i+1} - \frac{J}{2}\sum_{i=1}^{N}(\sigma_iS_i + \sigma_{i+1}S_{i+1}) \\ -\frac{\mu B}{2}\sum_{i=1}^{N}(\sigma_i + \sigma_{i+1}) - \frac{\mu B}{2}\sum_{i=1}^{N}(S_i + S_{i+1}) \quad (4.3)\end{aligned}$$

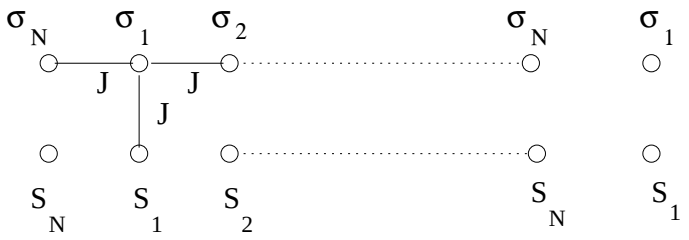

Figure 4.3: A linear double Ising chain. Spins in one the chain are denoted by σ and other by S. We use periodic boundary conditions. Any given spin is coupled to three nearest neighbours as shown.

We use periodic boundary conditions, so $\sigma_{N+1} \equiv \sigma_1$ and $S_{N+1} \equiv S_1$. The partition function of the system is given by

$$Z_N(B,T) = \sum_{\sigma_1, S_1 = \pm 1} \dots \sum_{\sigma_N, S_N = \pm 1} exp[\beta \sum_{i=1}^{N} \{J\sigma_i\sigma_{i+1} + JS_iS_{i+1} + \frac{J}{2}(\sigma_i S_i + \sigma_{i+1}S_{i+1}) + \frac{1}{2}\mu B(\sigma_i + \sigma_{i+1}) + \frac{1}{2}\mu B(S_i + S_{i+1})\}]$$

$$Z_N(B,T) = \sum_{\sigma_1, S_1 = \pm 1} \dots \sum_{\sigma_N, S_N = \pm 1} \langle \sigma_1, S_1 \mid T \mid \sigma_2, S_2 \rangle \langle \sigma_2, S_2 \mid T \mid \sigma_3, S_3 \rangle \dots \langle \sigma_{N-1}, S_{N-1} \mid T \mid \sigma_N, S_N \rangle \langle \sigma_N, S_N \mid T \mid \sigma_1, S_1 \rangle \quad (4.4)$$

where, T is called the transfer matrix. Explicitly,

$$T = \begin{pmatrix} e^{\beta(3J+2\mu B)} & e^{\beta\mu B} & e^{\beta\mu B} & e^{\beta J} \\ e^{\beta\mu B} & e^{-\beta J} & e^{-3\beta J} & e^{-\beta\mu B} \\ e^{\beta\mu B} & e^{-3\beta J} & e^{-\beta J} & e^{-\beta\mu B} \\ e^{\beta J} & e^{-\beta\mu B} & e^{-\beta\mu B} & e^{\beta(3J-2\mu B)} \end{pmatrix} \quad (4.5)$$

The summation over various σ_i and S_i in equation (4.11) lead to,

$$Z_N(B,T) = \sum_{\sigma_1, S_1 = \pm 1} \langle \sigma_1, S_1 \mid T^N \mid \sigma_1, S_1 \rangle = \mathrm{Tr}(T^N) = \lambda_1^N + \lambda_2^N + \lambda_3^N + \lambda_4^N \quad (4.6)$$

where, $\lambda_1, \lambda_2, \lambda_3, \lambda_4$ are eigenvalues of T. Thus all thermodynamic quantities of the linear double chain can be calculated for a specified set of parameters. Since the linear double chain is one dimensional, we do not expect magnetization at a finite temperature.

It would be of particular interest to look at the correlation length of the double chain. For a translationally invariant Hamiltonian, the relation between the correlation length ξ (in the units of lattice spacings) and eigenvalues is given by [33]

$$\xi^{-1} = ln(\lambda_1/\lambda_2) \quad (4.7)$$

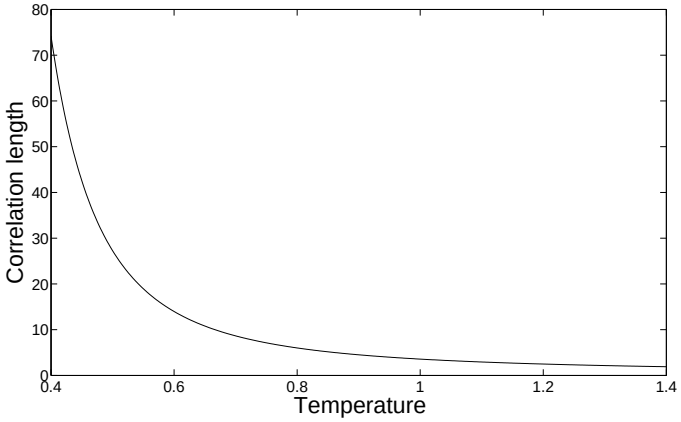

Figure 4.4: The correlation length (in units of lattice spacings) of linear double chain as a function of temperature.

where λ_1 is the largest eigenvalue of the transfer matrix T of the problem and λ_2 is the next largest.

Figure 4.4 gives the correlation length of the double Ising chain as a function of temperature. The comparative study of ordering in subsection 4.1.2 has been done at $T = 0.58$. The correlation length of the double chain at this temperature is about 15.7 lattice units.

4.2.2 Double chain with a kink

We now study a double chain with a kink. The presence of kink destroys the translational invariance of the problem. Without loss of generality we can assume that the kink is present at sites 2 and 3. Refer Figure 4.5. Periodic boundary conditions are employed as earlier. The transfer matrix elements at various sites can be written as below

$$\langle \sigma_1, S_1 \mid T_1 \mid \sigma_2, S_2 \rangle = exp[\beta\{\frac{J}{2}(\sigma_1 S_1 + \sigma_2 S_2) + J\sigma_1 S_2 + \frac{\mu B}{2}(\sigma_1 + \sigma_2) + \frac{\mu B}{2}(S_1 + S_2)\}] \tag{4.8}$$

$$\langle \sigma_2, S_2 \mid T_2 \mid \sigma_3, S_3 \rangle = exp[\beta\{J(\sigma_2\sigma_3 + S_2 S_3) + \frac{J}{2}(\sigma_2 S_2 + \sigma_3 S_3) + \frac{\mu B}{2}(\sigma_2 + \sigma_3) + \frac{\mu B}{2}(S_2 + S_3)\}] \tag{4.9}$$

$$\langle \sigma_3, S_3 \mid T_3 \mid \sigma_4, S_4 \rangle = exp[\beta\{\frac{J}{2}(\sigma_2 S_3 + \sigma_4 S_4) + J S_3\sigma_4 + \frac{\mu B}{2}(\sigma_3 + \sigma_4) + \frac{\mu B}{2}(S_3 + S_4)\}] \tag{4.10}$$

Comparing equation (4.9) with equation (4.3) it can be seen that the transfer matrix T_2 is same as the transfer matrix T. Hence, the partition function for the kinked chain can be written as,

$$Z_N(B,T) = \sum_{\sigma_1, S_1 = \pm 1} \dots \sum_{\sigma_N, S_N = \pm 1} \langle \sigma_1, S_1 \mid T_1 \mid \sigma_2, S_2 \rangle \langle \sigma_2, S_2 \mid T \mid \sigma_3, S_3 \rangle$$
$$\langle \sigma_3, S_3 \mid T_3 \mid \sigma_4, S_4 \rangle \langle \sigma_4, S_4 \mid T \mid \sigma_5, S_5 \rangle \dots \langle \sigma_N, S_N \mid T \mid \sigma_1, S_1 \rangle \tag{4.11}$$

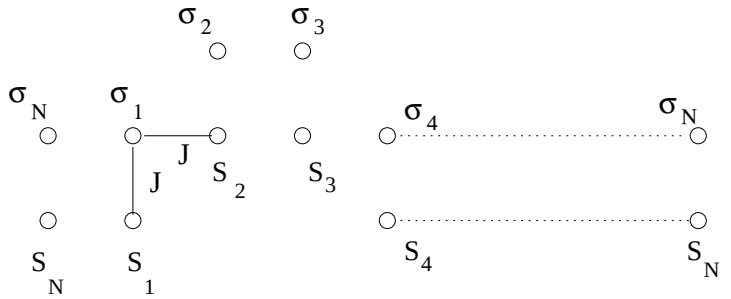

Figure 4.5: A chain with kink at sites 1 and 2.

Thus,

$$Z_N(B,T) = \mathrm{Tr}(T_1 T T_3 T^{N-3}) \tag{4.12}$$

Equation (4.12) is not as straight-forward to solve as equation (4.6). Nevertheless, it can be handled as follows.

Let $A = T_1 T T_3$. Using cyclic property of trace, $\mathrm{Tr}(AT^{N-3}) = \mathrm{Tr}(v_A^{-1} A T^{N-3} v_A)$. v_A is the matrix of eigenvectors of A and the transformation $v_A^{-1} A v_A$ diagonalizes A. So,

$$\begin{aligned} \mathrm{Tr}(AT^{N-3}) &= \mathrm{Tr}(\underline{v_A^{-1} A v_A} v_A^{-1} v_T \underline{v_T^{-1} T v_T} v_T^{-1} T \ldots v_T^{-1} T v_T v_T^{-1} v_A) \\ &= \mathrm{Tr}(D_A v_A^{-1} v_T D_T^{N-3} v_T^{-1} v_A) \end{aligned} \tag{4.13}$$

D_A and D_T are diagonal matrices with eigenvalues of A and T respectively as their diagonal elements. Equation (4.13) greatly reduces the computational cost associated with calculating the partition function for the kinked chain.

4.2.3 Quenched and Annealed averaging

The network along which have been studying ordering, Figure 3.1 C) can be thought as comprised of the linear double chain (Figure 4.3) and a kinked double chain (Figure 4.5). Let us assume that each one of them occurs with a probability p_1 and p_2 respectively. (Here onwards we shall denote the quantities, associated with double chain with subscript 1 and those associated with kinked chain with subscript 2).

The averaging over these two types of chains can be done in two ways.

Quenched averaging

The free energy is just the weighted sum of the individual free energies.

$$F_{quenched} = F_1 p_1 + F_2 p_2 \tag{4.14}$$

$$= -k_B T (p_1 ln Z_1 + p_2 ln Z_2) \tag{4.15}$$

The quenched averaging corresponds to a fixed network case introduced in section 4.1

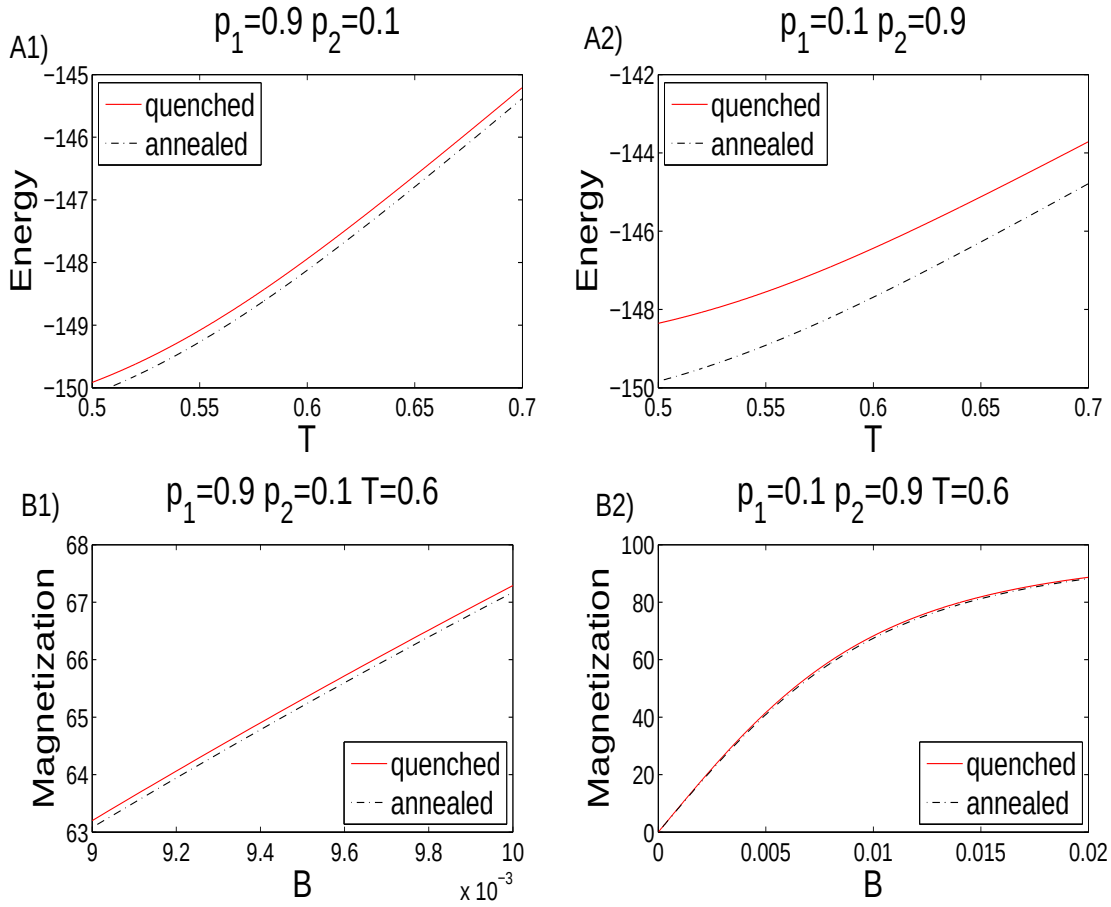

Figure 4.6: The top two graphs show the energy versus temperature graphs for the quenched and annealed averaging at magnetic field, $B = 0.01$.
The bottom two graphs show magnetization as a function of magnetic field at $T = 0.6$.

Annealed averaging

The annealed averaging corresponds to the dynamic network case in section 4.1. The partition function itself needs to be modified as, $Z_{annealed} = Z_1 p_1 + Z_2 p_2$. Therefore, the free energy is

$$F_{annealed} = -k_B T ln(Z_1 p_1 + Z_2 p_2) \tag{4.16}$$

We hope that by observing the properties such as internal energy, magnetization in a non-zero magnetic field in the above two cases could help us gain insight into the relative ordering between the fixed and dynamic network case in our actual system.

p_1 and p_2 can be related to the energy cost associated with creating kinks in the double chain. However, here we treat them as independent parameters and let them vary freely. [1]

[1] subject to the constraint that $p_1 + p_2 = 1$

Figure 4.6 shows that at a fixed temperature for a given magnetic field, the annealed averaging gives a slightly lesser value of magnetization compared to the quenched averaging. Thus, we might expect that in our system of interest, the dynamic network orders less than a fixed one does. We also observe that the change in probabilities, p_1 and p_2 does not affect the magnetization and energy behaviours qualitatively. We would expect that the system with less ordering has lower energy. However Figure 4.6 shows that annealed averaging has a lower energy. This needs to be understood.

Chapter 5

Discussions

It is evident from the results of simulations presented in Table 4.1 that we are unable to make a definite statement about the comparative ordering between the fixed and dynamic network case. Please note that this is in spite of having done long Monte Carlo runs over a large number of configurations. The analytical work in subsection 4.2.3 seems to suggest that a dynamical network would have a lower ordering. However, it is far from being foolproof. In this chapter we try to get some insights into the nature of our difficulty and propose methods to overcome them.

5.1 Numerical work

We start with the analysis of results presented in Table 4.1. To understand the relatively large value of standard deviation, we look at the trajectory the magnetization of a fixed network follows with time. Figure 5.1 shows that even for a static network, different realization of random numbers gives a widely different magnetization trajectory. This basically corresponds to long equilibriation time. It indicates that within the given time the system has not sampled its entire phase space.

The reason for the long equilibriation time can be attributed to the network geometry. The different segments of network get stuck in domains. Figure 5.2 shows snapshots of network during a run at two different time points. The domains are often connected by just one spin. Thus the energy cost associated with formation of such domains is less. Most of the times, the spins on the domain boundary are satisfied, in the sense that majority of its neighbours point in the same direction as itself and is reluctant to flip. This leads to long life-time of the domains.

Nevertheless, if run for sufficiently long time all points in the phase space would be sampled and we could get a accurate estimate. A long run is equivalent to many short runs. From equation (4.1) we know that the error decreases as $1/\sqrt{n}$. Thus, from Table 4.1 to get an error of 0.001 we need to make about 2800 runs. With the computational resources at our disposal, it takes around 15 days for 80 runs. So, it will take 525 days for 2800 runs. Clearly the task is beyond the scope of this project. Nonetheless, in principle it can always be done, perhaps with a help of faster computer.

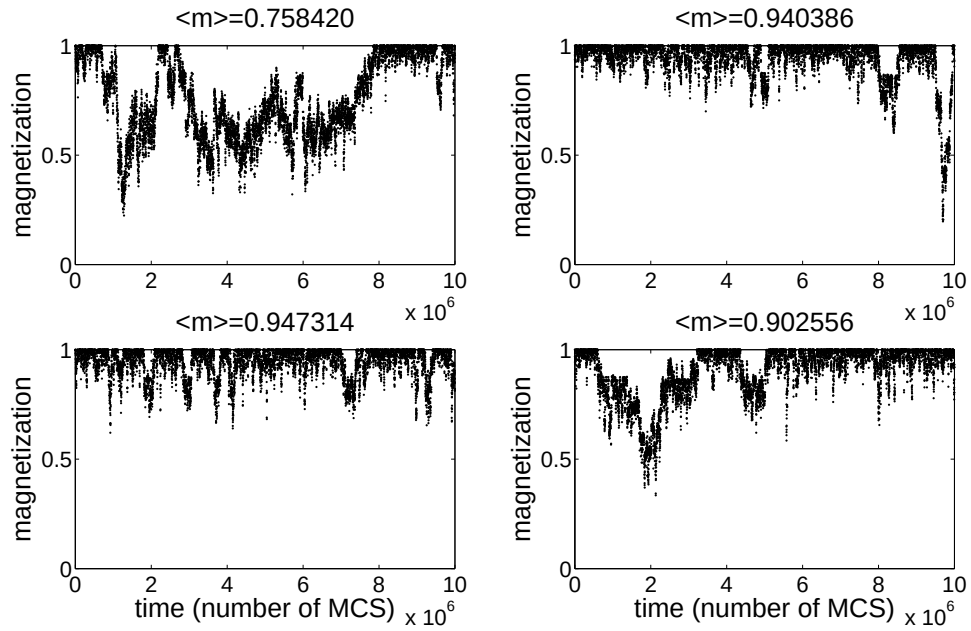

Figure 5.1: The runs are performed with same initial condition at $T = 0.58$. The different realizations of random number generator give different magnetization trajectories.

5.2 Analytical Work

The approach of quenched and annealed averaging introduced in subsection **??** can be extended further. For instance, we can take into account that our system also consists of chains with two kinks, three kinks and so on. Hence, there is scope to build up the level of complexity and gain better understanding of the underlying physics.

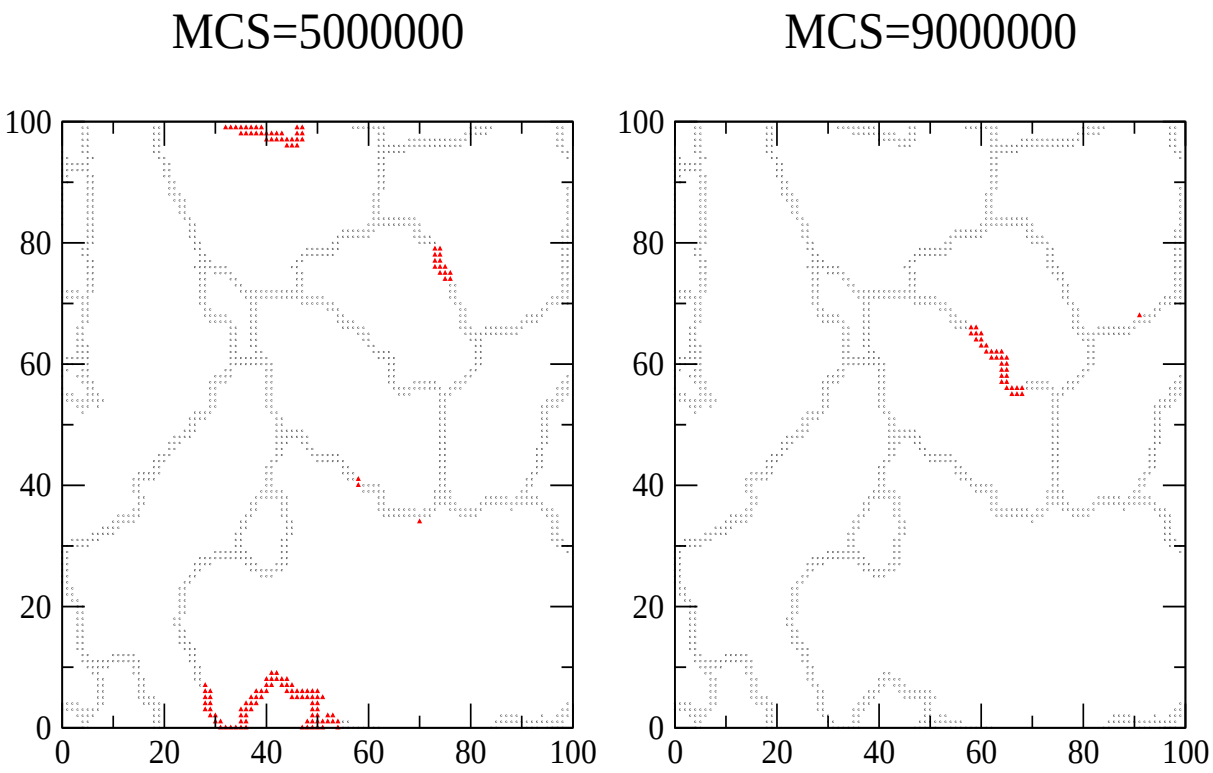

Figure 5.2: The network configurations at two time points. The up and down spins are indicated by • and △ respectively

References

[1] Legget, A. J. Rev. Mod. Physics **71** (1999) S318.

[2] London, F. Superfluids (Wiley, New York, 1950).

[3] Landau, L. Phys. Rev. **60** (1941) 356.

[4] Feynman, R. P., Progress in Low Temperature Physics, **1** (1955) 17.

[5] Penrose, O. and Onsager, L. Phys. Rev. **104** (1956) 576.

[6] Legget, A. J. Quantum Liquids (Oxford University Press, 2006).

[7] Chester, G. V. Phys. Rev A **2** (1970) 256

[8] Kim, E. and Chan, M. H. W. Nature **427** (2004) 225.

[9] Kim, E. and Chan, M. H. W. Science **305** (2004) 1941.

[10] Chalmers, Matthew. Physics World (2007).

[11] Day, J. and Beamish J. Nature **450** (2007) 853.

[12] Mukharsky, Yu., Penzev, A. and Varoquaux, E. Phys. Rev. B **80** (2009) 140504.

[13] Lin, X., Clark, A. C., Cheng, Z. G. and Chan, M. H. W. Phys. Rev. Lett. **102** (2009) 125302.

[14] Balibar, Sebastien. Nature **464** (2010) 176.

[15] Thouless, D. J. Ann. Phys. **52** (1969) 403.

[16] Andreev, A. F. and Lifshitz, I. M. Sov. Phys. JETP **29** (1969) 1107.

[17] Prokof'ev, N. Adv. Phys. **56** (2007) 381.

[18] Ceperley, D. M. and Bernu, B. Phy. Rev. Lett. **93** (2004) 155303.

[19] Rittner, A. S. and Reppy, J. Phys. Rev. Lett. **98** (2007) 175302.

[20] Kim E, Xia J S, West J T, Lin X, Clark A C and Chan M H W Phys. Rev. Lett. **100** (2008) 065301.

[21] Anderson, P. W. Phys. Rev. Lett. **100** (2008) 215301.

[22] Balibar Sébastien and Frédéric Caupin. J Phys: Cond Mat **20** (2008) 173201.

[23] Ashkin, J. and Teller, E. Phys. Rev. **64**, (1943) 178.

[24] Ditzian et al. Phys. Rev B **22** (1980) 2542.

[25] Baxter, R. J. Exactly Solved Models in Statistical Mechanics (Academic Press).

[26] Press et al. - Numerical Recipes in C: The Art of Scientific Computing. (Cambridge University Press)

[27] Binny J. J. et al. - The Theory of Critical Phenomena: An Introduction to Renormalization Group. (Oxford University Press, 1992)

[28] Potts, R. B. Proc. Camb. Phil. Soc. **48** (1952) 106.

[29] Wu, F. Y Rev. Mod. Physics **54** (1982) 235.

[30] Lukierska-Walasek K. and Topolski K. Rev. Adv. Mater. Sci. **23** (2010) 141-146

[31] Kramers, H. A and Wannier, G. H. Phys. Rev. **60** (1941) 252

[32] Pathria, R. K. - Statistical Mechanics (Elsevier).

[33] Yeomans, J - Statistical Mechanics of phase transitions (Oxford University Press, 1992).

[34] Ross, Sheldon M - Introduction to Probability Models (Academic Press).

Appendix A

Long proofs

A.1 Derivation of Mean Field equations

The mean field Hamiltonian is defined in terms of self consistent field as,

$$\mathcal{H}_{MF} = -h_{\sigma_A}\sum_A \sigma - h_{S_A}\sum_A S - h_{\sigma_B}\sum_B \sigma - h_{S_B}\sum_B S \tag{A.1}$$

h_{σ_A},h_{S_A},h_{σ_B},h_{S_B} are the self consistent field to be determined from the minimization of the variational free energy.

The variational free energy as explained in [27] is given by,

$$F_{var} = \langle\mathcal{H}\rangle - \langle\mathcal{H}_{MF}\rangle - k_B T ln Z_{MF} \tag{A.2}$$

$$\langle\mathcal{H}\rangle = -J_1\sum_{\langle i,j\rangle}\langle\sigma\rangle_A\langle\sigma\rangle_B - \frac{J_2}{2}\sum_{\langle i,j\rangle}\langle S\rangle_A\langle S\rangle_B + \frac{J_2}{2}\sum_{\langle i,j\rangle}\langle\sigma\rangle_A\langle S\rangle_A\langle\sigma\rangle_B\langle S\rangle_B$$

$$\langle\mathcal{H}_{MF}\rangle = -h_{\sigma_A}\langle\sigma\rangle_A\frac{N}{2} - h_{S_A}\langle S\rangle_A\frac{N}{2} - h_{\sigma_B}\langle\sigma\rangle_B\frac{N}{2} - h_{S_B}\langle S\rangle_B\frac{N}{2}$$

Putting this in equation (A.2) and using the condition, $\frac{dF_{var}}{dh_{\sigma_A}} = 0$, we get,

$$h_{\sigma_A} = 4J_1\langle\sigma\rangle_B - 2J_2\langle S\rangle_A\langle S\rangle_B\langle\sigma\rangle_B \tag{A.3}$$

We have used here $\langle\sigma\rangle_A = \frac{1}{N/2}k_B T\frac{dlnZ_{MF}}{dh_{\sigma_A}}$ [1]

Following similar lines, the other three self consistent fields turn out to be,

$$h_{\sigma_B} = 4J_1\langle\sigma\rangle_A - 2J_2\langle S\rangle_A\langle S\rangle_B\langle\sigma\rangle_A \tag{A.4a}$$
$$h_{S_A} = 2J_2\langle S\rangle_B - 2J_2\langle\sigma\rangle_A\langle\sigma\rangle_B\langle S\rangle_B \tag{A.4b}$$
$$h_{S_B} = 2J_2\langle S\rangle_A - 2J_2\langle\sigma\rangle_A\langle\sigma\rangle_B\langle S\rangle_A \tag{A.4c}$$
$$\tag{A.4d}$$

[1] We consider that total system has size N, so each sublattice will have $N/2$ spins.

Now,

$$\begin{aligned}\langle\sigma\rangle_A = &\quad \frac{\sum \sigma_{i_A} e^{-\beta H_{MF}}}{\sum e^{-\beta H_{MF}}} \\ = &\quad \frac{\sum \sigma_{i_A} e^{\beta h_{\sigma_A} \sum \sigma_{i_A}}}{\sum e^{\beta h_{\sigma_A} \sum \sigma_{i_A}}} \\ = &\quad tanh(\beta h_{\sigma_A})\end{aligned}$$

Similarly, we have, $\langle\sigma\rangle_B = tanh(\beta h_{\sigma_B})$ and $\langle S\rangle_{A,B} = tanh(\beta h_{S_{A,B}})$. Inserting the expression for mean fields (equation (A.4)), we recover the equations (2.3) studied in section 2.2

Appendix B

Short proofs

B.1 Proof of the theorem (4.1) invoked in subsec. 4.1.2

To prove equation (4.1), we use the fact that the average or expectation value is a linear function. So,

$$E(aX + b) = aE(X) + b \tag{B.1}$$

The proof of equation (B.1) is quite straight forward and for instance can be found in [34].

Now,

$$\begin{aligned} \mathrm{Var}[aX + b] &= E[(aX + b)^2] - [E(aX + b)]^2 && \text{(B.2)} \\ &= E(a^2X^2 + 2aXb + b^2) - [aE(X) + b]^2 \\ &= a^2(E(X^2) - E(X)^2) = a^2\mathrm{Var}(X) && \text{(B.3)} \end{aligned}$$

For N independent and identically distributed random variables, $X_1, X_2, \ldots, X_N$

$$\begin{aligned} \mathrm{Var}(\bar{X}) &= \mathrm{Var}(\sum_{i=1}^{N} \frac{X_i}{N}) \\ &= \frac{1}{N^2} \sum \mathrm{Var}(X_i) = \frac{1}{N^2} N\sigma^2 = \frac{\sigma^2}{N} && \text{(B.4)} \end{aligned}$$

Thus,

$$std(\bar{X}) = \frac{\sigma}{\sqrt{N}} \tag{B.5}$$

Hence, proved.